ISSN 1990-7931, Russian Journal of Physical Chemistry B, 2023, Vol. 17, No. 3, pp. 658–672. © Pleiades Publishing, Ltd., 2023.

STRUCTURE OF CHEMICAL COMPOUNDS, QUANTUM CHEMISTRY, SPECTROSCOPY

Electric and Magnetic Evaluation of Aluminum–Magnesium Nanoalloy Decorated with Germanium Through Heterocyclic Carbenes Adsorption: A Density Functional Theory Study

F. Mollaamin[a, *] and M. Monajjemi[b]

[a] *Department of Food Engineering, Faculty of Engineering and Architecture, Kastamonu University, Kastamonu, Turkey*
[b] *Department of Chemical Engineering, Central Tehran Branch, Islamic Azad University, Tehran, Iran*
**e-mail: smollaamin@gmail.com*

Received January 3, 2023; revised March 8, 2023; accepted March 20, 2023

Abstract—Heterocyclic compounds with multiple bonds and heteroatoms of nitrogen, oxygen and sulfur can be notable as corrosion inhibitors for metal surfaces. In this work, Ge-doped Al–Mg nanoalloy has been investigated based on Langmuir adsorption and density functional theorey method (DFT) method. The partial electron density states (PDOS) have confirmed an obvious charge accumulation between the Al–Mg alloy and doped atom of Ge through the recognition of the conduction band region. The infrared (IR) spectrums for complexes of inhibitors adorbed on Ge-doped Al–Mg alloy have been reported in the frequency between 500–3500 cm^{-1} for (benzotriazole/2-mercaptobenzothiazole/8-hydroxyquinoline) → Al–Mg–Ge, and around 500–4000 cm^{-1} for 3-amino-1,2,4-triazole-5-thiol → Al–Mg–Ge with the sharpest peak approximately around 2000 cm^{-1}, 3000 cm^{-1} for (benzotriazole/2-mercaptobenzothiazole/8-hydroxyquinoline) → Al–Mg–Ge and 2000 cm^{-1}, and 4000 cm^{-1} for 3-amino-1,2,4-triazole-5-thiol → Al–Mg–Ge. Nuclear magnetic reonance (NMR) spectrocopy has focused on the intra-atomic and interatomic interactions with ONIOM model with three levels of high, medium and low by using LANL2DZ/6-31+G(*d*, *p*), semi-empirical and MM2 functions. Al–Ge(14), Al–Ge(19) and Al–Ge(21) in the Al–Mg–Ge alloy surface with the highest fluctuation in the shielding tensors of NMR spectrums generated by intra-atomic interaction direct us to the most influence in the neighbor atoms generated by interatomic reactions of N → Al, O → Al, S → Al through the coating and adsorbing process of Langmuir adsorption. This work indicated that proper monitoring of the coating mechanism by Langmuir adsorption can illustrate inhibiting the ternary aluminum nanoalloy of Al–Mg–Ge corrosion through an investigation of their structural and physicochemical analysis. Furthermore, it has been illusstrated the effect of the substitution of aluminum atoms in Al–Al nanosheet with Mg and Ge through resulted electric potential by using Nuclear quadrupole resonance (NQR) analysis.

Keywords: DFT, Al–Mg–Ge, Langmuir adsorption, benzotriazole, 2-mercaptobenzothiazole, 8-hydroxyquinoline, 3-amino-1,2,4-triazole-5-thiol

DOI: 10.1134/S1990793123030223

INTRODUCTION

The adsorption of heterocyclic compounds on the metal surface closes active zones and decreases the speed of corrosion. Nevertheless, the efficiency of the inhibitor is related to the physicochemical attributes such as inhibitor structure, being special functional groups, aromaticity, different types of corrosive solutions and charge electron density [1–4].

Al–Mg–Ge alloy displays qualitatively the identical evolution of positron lifetime τ1C with time as Al–Mg–Si alloy, as a primary reduction, pursued by a re-enhancement, after which τ1C falls to an equilibrium amount. But, for alloys with identical magnesium contents, germanium gives increase to a remarkably slower ageing kinetics than silicon, because of impacts of atomic binding energies. Increasing copper to both Al–Mg–Ge and Al–Mg–Si alloys calms down the primary configuration of complexes but develops their further outcome [5–11].

The alloys of aluminum are formed by the special alloying elements such as Cu, Mg, Mn, Si, Sn, Ni and Zn. Light weight or corrosion resistance of aluminum alloys make them suitable in engineering structures and components. Aluminum-silicon (Al–Si) is one of the most important aluminum alloys with high amounts of silicon in casting and has a large limitation of usages in the aerospace and automotive industries through a best combination of mechanical properties, as well as good wear resistivity and corrosion resistance [12–14]. Si element in Al–Si based cast alloys impacts tensile properties at both room and high temperature, but its role becomes more important in lack of alloy elements such as Mg, Fe and Cu [15]. Some

elements like Cu and Mg added to Al alloys ameliorate the mechanical attributes and conduct the alloy to reply the heat dealing. The existence of magnesium also increases resistance and reduces the rate of strength loss at high temperature in the alloys. Aluminum-magnesium (Al–Mg) alloys are lighter than other aluminum alloys and much less flammable than other alloys consisting of high amounts of magnesium. The magnificent enhancement in resistance at elevated temperature was accomplished after solution treatment through activating settlement becoming hard through Mg possessing phases.

Among the various methods that minimize corrosion of metal surface, its inhibition by organic molecules is one of the most applicable methods because of its stability and low cost [16–20]. There are many researches that have been dedicated to the application of efficient heterocyclic and heteroatomic including organic compounds that ameliorate the anticorrosion attributes of metal surfaces and alloys. The existence of heteroatoms containing O, S, N, P atoms, aromatic rings and multiple bonds with π-electrons in these inhibitors help extensively to the formation of inactive blocks on metal surface and alloys, so closing the active sites of corrosion [21–27].

Based on some researches, benzotriazole, 2-mercaptobenzothiazole, 8-hydroxyquinoline, and 3-amino-1,2,4-triazole-5-thiol are organic cyclic inhibitors for metal, semi-metals or non-metals surfaces and their alloys by preventing undesirable surface reactions. It is obvious that a passive layer, containing a complex between surface and these inhibitors, is generated when surface is immersed in a solution consisting of benzotriazole, 2-mercaptobenzothiazole, 8-hydroxyquinoline, and 3-amino-1,2,4-triazole-5-thiol. The passive layer is insoluble in aqueous and many organic solutions. There is a positive connection between the thickness of the passive layer and the efficiency of preventing corrosion [28–30].

In the previous works, the adsorption analysis of pyridine, and nitrogen heterocyclic derivatives onto pristine two-layer aluminum surface [31], pure monolayer aluminum metal surface based on Freundlich Adsorption [32] have been investigated. Moreover, the results of Langmuir adsorption model of organic inhibitors containing benzotriazole, 8-hydroxyquinoline, and 2-mercaptobenzothiazole by using monolayer binary alloys of the Al–Mg, Al–Ga, Al–Si surfaces have been reported [33]. The present work intend to investigate the role of benzotriazole, 2-mercaptobenzothiazole, 8-hydroxyquinoline, and 3-amino-1,2,4-triazole-5-thiol as corrosion inhibitors for monolayer ternary aluminum nanoalloy which has been generated by adding some germanium and magnesium elements to Al-surface and forming the Al–Mg–Ge nanoalloy.

MATERIALS AND METHOD

In this research, it has been attributed the inhibiting effect of the benzotriazole, 2-mercaptobenzothiazole, 8-hydroxyquinoline, and 3-amino-1,2,4-triazole-5-thiol on the adsorption through a stable complex formed on the aluminum alloy of Al–Mg–Ge surface.

The verdict dealing with the influence of the heterocyclic inhibitors in solution and the nature of the corrosive aluminum alloys on the adsorption bond strength yields information about the mechanism of interaction of the inhibitor with the Al alloys surface, which in turn Langmuir adsorption isotherms provide excellently. The Langmuir isotherm is widely used in the identification of inhibitor adsorption status specification and it is represented as follows [34]:

$$\frac{C_{\text{inh}}}{\theta} = \frac{1}{K_{\text{ads}}} + C_{\text{inh}}, \quad (1)$$

where C_{inh} is the inhibitor concentration; θ is the fractional coverage of the steel surface and K_{ads} is the equilibrium constant of the adsorption and desorption procedures.

Using the Langmuir isotherm, the equilibrium constant of adsorption and desorption procedures (K_{ads}) could be specified and depends on the standard free energy of adsorption $\Delta G^{\circ}_{\text{ads}}$ as follows [35]:

$$\Delta G^{\circ}_{\text{ads}} = -RT\left(55.5K_{\text{ads}}\right), \quad (2)$$

where R is the gas constant (8314 J K^{-1} mol^{-1}), T is the absolute temperature (T) and the value 55.55 (mol^{-1}) is the concentration of water in solution.

The adsorption of benzotriazole, 2-mercaptobenzothiazole, 8-hydroxyquinoline, and 3-amino-1,2,4-triazole-5-thiol as corrosion inhibitors on the aluminum alloy surface of Al–Mg–Ge in NaCl solution was assigned by the most suitable Langmuir isotherm, which exhibits the chemisorptive nature of the bond between the inhibitor molecules and the Al–Mg–Ge alloy surface, the equilibrium distribution of ions of the adsorbing compound between the solid and liquid phases, and a monolayer attribute.

The adsorbed molecules are kept on the Al–Mg–Ge alloy surface with chemisorbed inhibitors having high protection (Fig. 1).

In this research, the combination of three levels of ONIOM method in decreasing order of accuracy is defined including high, medium, and low levels of theory. High-level has been done using the DFT method of Cam-B3LYP with 6-31+G(d, p) basis set for some hydrogen, carbon, oxygen, and sulfur and also some germanium atoms in the adsorption site, EPR-III basis set for nitrogen and LANL2DZ for some aluminum and magnesium atoms in the adsorption cites. Medium-level has been done on the hydrogen, carbon, nitrogen, oxygen, sulfur in the adsorption

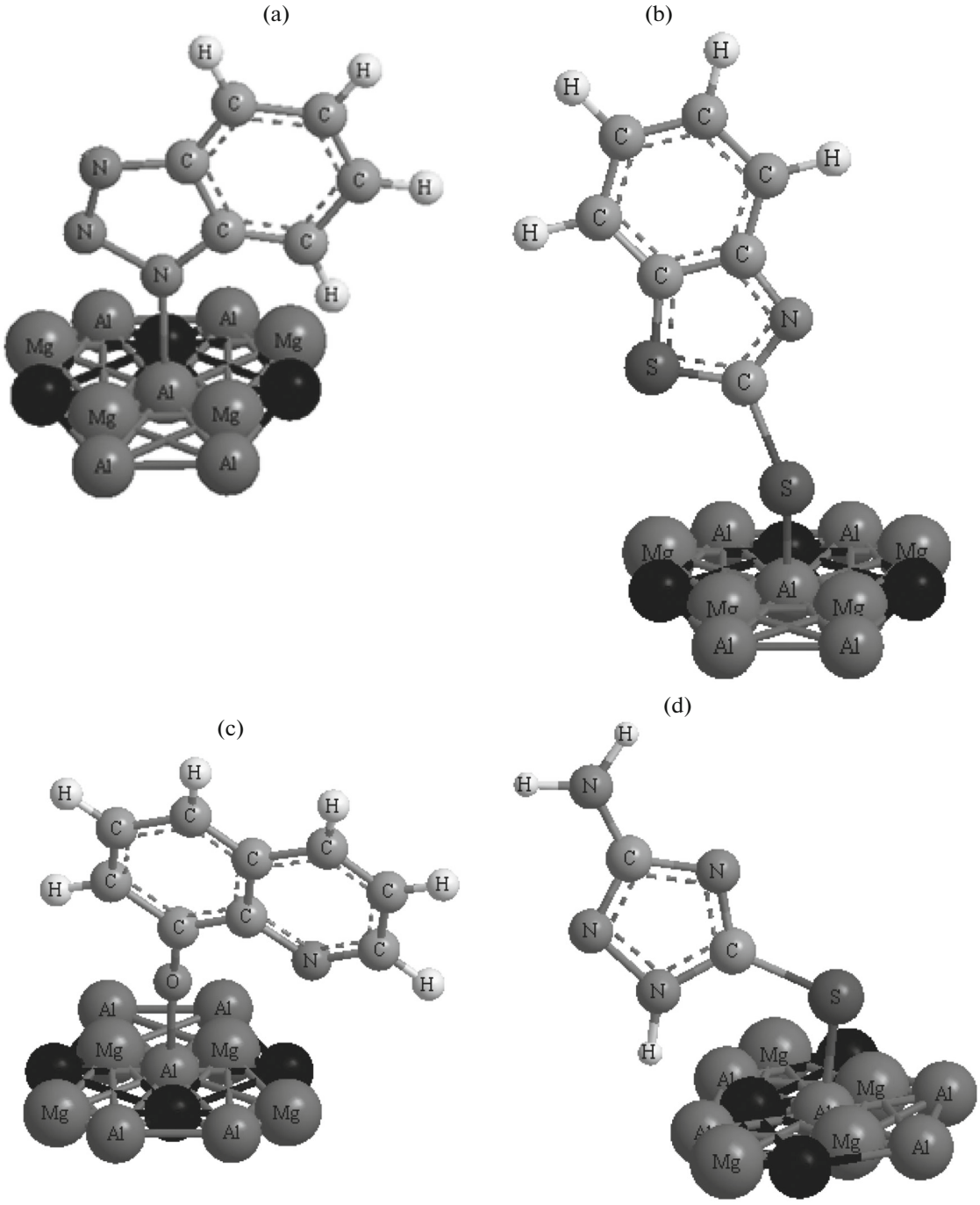

Fig. 1. Langmuir adsorption of the organic corrosion inhibitors of (a) benzotriazole, (b) 2-mercaptobenzothiazole, (c) 8-hydroxyquinoline, (d) 3-amino-1,2,4-triazole-5-thiol onto Ge-doped on Al–Mg nanoalloy (black sphere is Ge).

sites due to semi-empirical methods. Finally, a low-level has been performed on the other aluminum, magnesium, and germanium atoms with MM2 force fields (Fig. 2) [36]:

$$E_{\mathrm{ONIOM}} = E_{\mathrm{High}} + E_{\mathrm{Medium}} + E_{\mathrm{Low}}. \quad (3)$$

On the other hand, the three-layered method of ONIOM lets us to discover a larger system more exactly than the one-layered model which could behave a medium size system precisely like a ground system with acceptable accuracy [37].

Therefore, this three-layered pattern has been applied for effective barriers of benzotriazole, 2-mercaptobenzothiazole, 8-hydroxyquinoline, and 3-amino-1,2,4-triazole-5-thiol adsorbing onto Al–Mg–Ge alloy surface (Fig. 2).

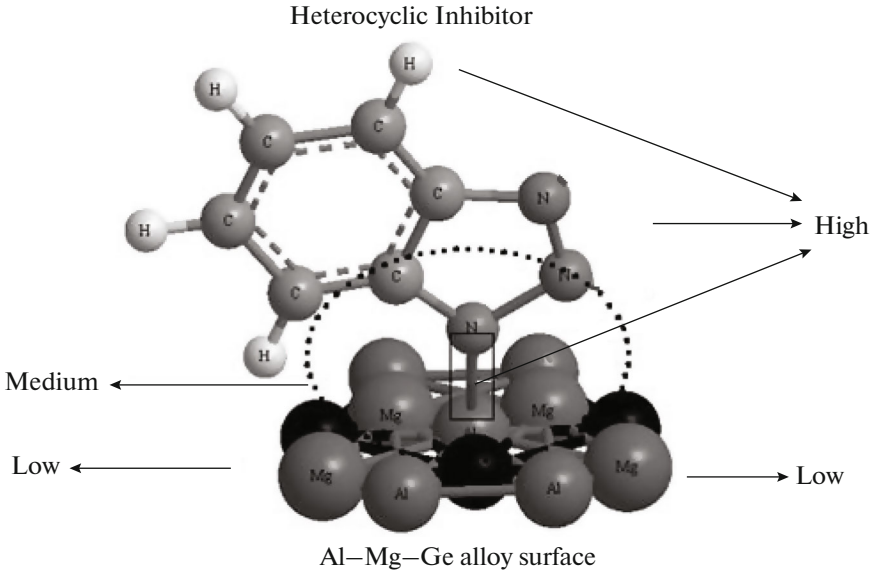

Fig. 2. The ONIOM layer of adsorption mechanism for 3-amino-1,2,4-triazole-5-thiol as a corrosion inhibitor onto Al–Mg–Ge alloy surface based on optimized coordination.

It has been calculated the structures using the density functional theory (DFT) on the mechanisms onto Al–Mg–Ge alloy surface up to adsorbed in the active sites of heterocyclic inhibitors by nitrogen, oxygen and sulfur atoms of benzotriazole, 8-hydroxyquinoline, 2-mercaptobenzothiazole, and 3-amino-1,2,4-triazole-5-thiol, respectively.

It has been found that the surface binding site preferences of N-atom of benzotriazole, O-atom of 8-hydroxyquinoline and S-atom of both of 2-mercaptobenzothiazole and 3-amino-1,2,4-triazole-5-thiol in adsorption site is largely affected by the presence of neighboring atoms. The calculated N → Al, O → Al and S → Al pair distribution functions have indicated that the formation of clusters directs to shorter N → Al, O → Al and S → Al bond lengths when compared to the homogeneous growth (Fig. 2).

In this work, atomic structure of the Al–Mg–Ge alloy surface has been built using GaussView 6.06.16 [38] and calculated by Gaussian 16 revision C.01 software [39] through geometry coordination. Result observations have represented that the Al–Mg–Ge alloy surface calculated with the achieved structure parameters are in good agreement with those metal alloys attained from other experimental calculations [40–45].

Hybrid functional is a group of approximations for the exchange-correlation energy functional in DFT (Density Functional Theory) which combines a part of exact exchange from HF (Hartree–Fock theory) method with the rest of the exchange-correlation energy from other information such as empirical or ab initio methodologies. Therefore, the exact exchange energy functional is illustrated by the Kohn–Sham orbitals instead of the density, so is placed as the indirect density functional. This study has applied the influence of the hybrid functional of three-parameter basis set of B3LYP (Becke, Lee, Yang, Parr) within the framework of DFT upon theoretical calculations [46, 47]. In fact, the popular B3LYP (Becke, three-parameter, Lee–Yang–Parr) exchange-correlation functional is [48–50]:

$$E_{\mathrm{XC}}^{\mathrm{B3LYP}} = (1-\alpha)E_{\mathrm{x}}^{\mathrm{LSDA}} + \alpha E_{x}^{\mathrm{HF}} + b\Delta E_{x}^{\mathrm{B}} + (1-c)E_{\mathrm{c}}^{\mathrm{LSDA}} + cE_{\mathrm{c}}^{\mathrm{LYP}}, \quad (4)$$

where $\alpha = 0.20$, $b = 0.72$, $c = 0.81$ is a generalized gradient approximation: the Becke exchange functional [36] and the correlation functional of Lee, Yang and Parr [37] for B3LYP and $E_{\mathrm{c}}^{\mathrm{LSDA}}$ is the VWN local spin density approximation to the correlation functional [51].

The Al–Mg–Ge alloy surface has been built by rigid system and Z-Matrix format of which a blank line has been placed and after that the following information has been illustrated. The rigid PES has been performed at CAM-B3LYP functional [52], and employing 6-31+G(*d*, *p*)/EPR-III/LANL2DZ basis sets to assign atomic charges, nuclear magnetic resonance properties, dipole moment, thermodynamic characteristics and other quantum properties in this study [53] for benzotriazole, 8-hydroxyquinoline, 2-mercaptobenzothiazole, and 3-amino-1,2,4-triazole-5-thiol adsorbing onto the Al–Mg–Ge alloy surface using Gaussian 16 revision C.01 software [39]. The input files for the heterocyclic corrosion inhibitors of adsorbed onto Al–Mg–Ge surface has been provided with GaussView 6.06.16 [38]. For Al-alloy surface, the

Table 1. The physico-chemical properties of adsorption for benzotriazole, 2-mercaptobenzothiazole, 8-hydroxyquinoline, and 3-amino-1,2,4-triazole-5-thiol as corrosion inhibitors on the aluminum alloy surface of Al–Mg–Ge in NaCl solution at 300 K

Compound	$\Delta H^\circ \times 10^{-4}$, kcal/mol	$\Delta G^\circ \times 10^{-4}$, kcal/mol	S°, cal/K mol	Dipole moment, Db
Al–Mg–Ge	–512.93	–512.93	79.09	1.53
Benzotriazole	–24.51	–24.52	80.25	3.31
Benzotriazole → Al–Mg–Ge	–534.65	–534.65	91.30	4.86
2-Mercaptobenzothiazole	–69.52	–69.52	85.64	2.51
2-Mercaptobenzothiazole → Al–Mg–Ge	–579.64	–579.64	94.59	3.14
8-Hydroxyquinoline	–29.55	–29.55	83.33	1.64
8-Hydroxyquinoline → Al–Mg–Ge	–539.70	–539.70	94.44	2.12
3-Amino-1,2,4-triazole-5-thiol	–43.13	–43.13	73.84	1.56
3-Amino-1,2,4-triazole-5-thiol → Al–Mg–Ge	–553.26	–553.26	90.82	2.21

small energy difference between the formations of inhibitor → Al–Mg–Ge alloy complex can direct us to a pretty coated surface for preventing the corrosion.

RESULTS AND DISCUSSION

In this article, the susceptibility of heterocyclic inhibitors including benzotriazole, 2-mercaptobenzothiazole, 8-hydroxyquinoline, and 3-amino-1,2,4-triazole-5-thiol characteristics of aluminum alloy surface (Al–Mg–Ge) and adsorption conditions have been illustrated.

The electronic structures of Al–Al, Al–Mg and Al–Mg–Ge surfaces have been analyzed to simplify subsequent discussion for interfacial electronic properties through projection of particular orbital of particular atom on the density of states (PDOS) by using density functional theory (DFT) and LANL2DZ basis set. The PDOS has described the orbital states of pristine Al-Al surface, binary Al–Mg alloy and the rate of dominancy of Ge-doped on the Al–Mg alloy by forming ternary Al–Mg–Ge surface through the conduction band (Fig. 3). A distinct metallic feature can be observed in the Al–Mg–Ge alloy because of the strong interaction between the *p* states of Al and the *d* states of Ge close to the Fermi energy. In addition, the presence of covalent features for this alloy has exhibited the identical energy amount and figure of the PDOS for the *p* orbitals of Al and *d* orbitals of Ge.

Figure 3a has shown that the Al states in the Al–Al alloy have more contribution at the middle of the conduction band between –5 to –15 eV. Al and Mg states in the Al–Mg alloy have similar contributions at the middle of the conduction band between –5 to –15 eV, while contribution of Al states are weaker than Mg states (Fig. 3b). But, Ge states in the Al–Mg–Ge alloy reveal the expanded contribution with the conduction band between –1 to –20 eV, while Mg states are stronger than Al and Ge states (Fig. 3c).

The results also are approved by the partial electron density (PDOS), which have showed a certain charge association between the Al–Mg alloy and doped of Ge element. In other words, the Mg states have large contributions in the valence band, while Ge and Al states have less contribution. Thus, the above results exhibit that the cluster dominant of metallic feature and a certain degree of covalent trait can illustrate the increasing of the semiconducting direct band gap of Ge-doped on the Al–Mg alloy.

The infreared (IR) spectrums for each of these compounds has been seen in the frequency range around 500–3500 cm^{-1} for benzotriazole → Al–Mg–Ge, 2-mercaptobenzothiazole → Al–Mg–Ge, and 8-hydroxyquinoline → Al–Mg–Ge; 500–4000 for 3-amino-1,2,4-triazole-5-thiol → Al–Mg–Ge with the sharpest peak approximately around 2000 cm^{-1}, 3000 cm^{-1} for benzotriazole → Al–Mg–Ge, 2-mercaptobenzothiazole → Al–Mg–Ge, and 8-hydroxyquinoline → Al–Mg–Ge; 2000, 4000 cm^{-1} for 3-amino-1,2,4-triazole-5-thiol → Al–Mg–Ge (Fig. 4).

The infrared (IR) calculations have been accomplished for aluminum alloy of Al–Mg–Ge interacting with four heterocyclic inhibitors including benzotriazole, 2-mercaptobenzothiazole, 8-hydroxyquinoline, and 3-amino-1,2,4-triazole-5-thiol adsorbed onto this alloy surface which produce the complexes of benzotriazole → Al–Mg–Ge, 2-mercaptobenzothiazole→ Al–Mg–Ge, 8-hydroxyquinoline → Al–Mg–Ge, and 3-amino-1,2,4-triazole-5-thiol → Al–Mg–Ge at CAM-B3LYP level of theory employing 6-31+G(*d*, *p*)/EPR-III/LANL2DZ basis sets to obtain the more accurate equilibrium geometrical parameters, physical and thermodynamic properties for each of the determined structure (Table 1).

From Fig. 5, it could be found that the maximum of the Langmuir adsorption isotherm plots based on ΔG°_{ads} may depend on the interactions between the inhibitor structures and the Al–Mg–Ge nanoalloy

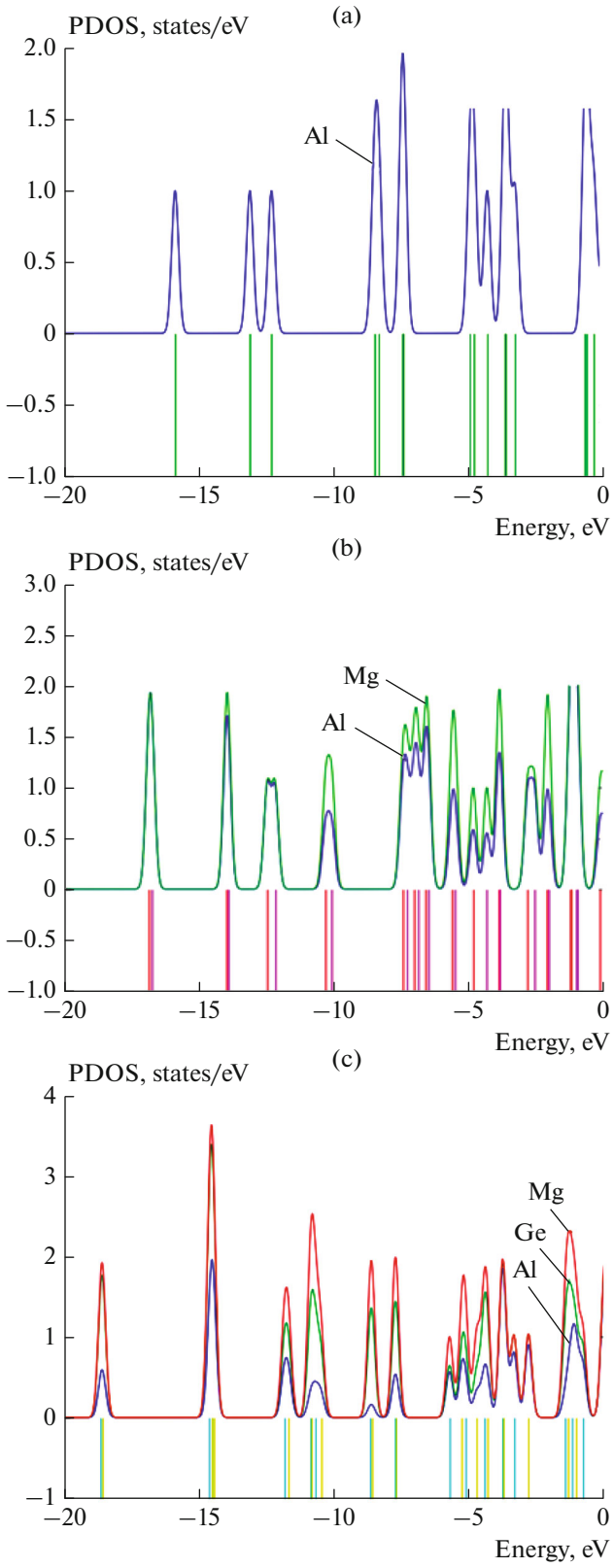

Fig. 3. PDOS of (a) Al–Al, (b) Al–Mg and (c) Al–Mg–Ge nanoalloys with Fermi level equal to 0.

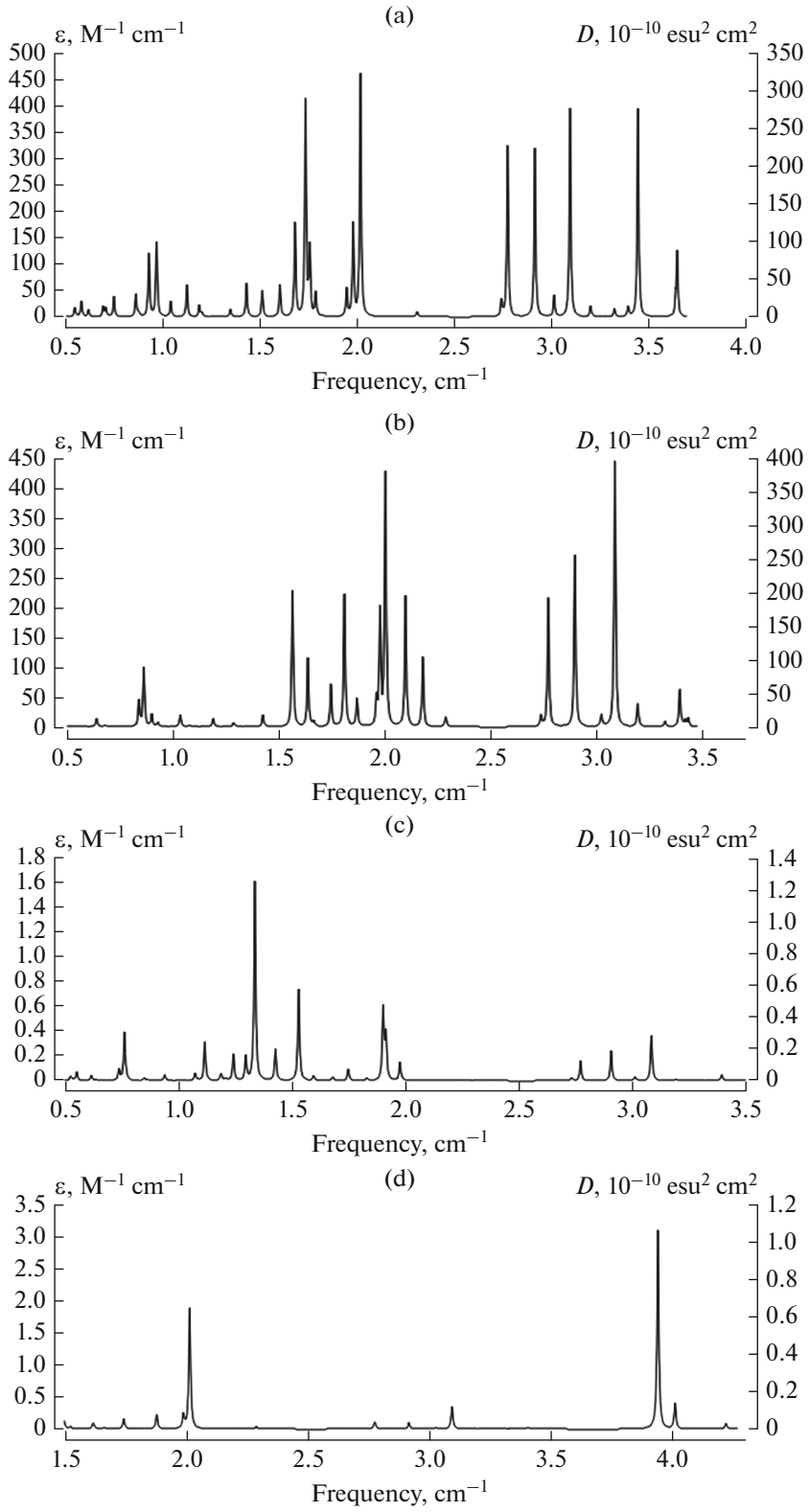

Fig. 4. Changes of frequency (cm^{-1}) through the IR spectra for (a) benzotriazole → Al–Mg–Ge, (b) 2-mercaptobenzothiazole → Al–Mg–Ge, (c) 8-hydroxyquinoline → Al–Mg–Ge, and (d) 3-amino-1,2,4-triazole-5-thiol → Al–Mg–Ge using CAM-B3LYP method with 6-31+G(*d*, *p*)/EPR-III/LANL2DZ basis sets.

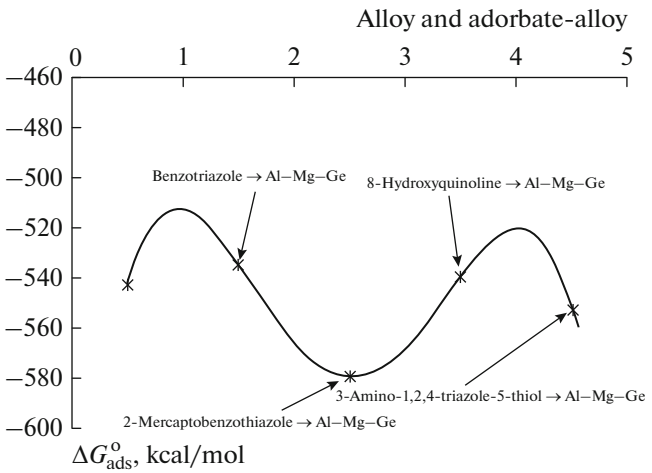

Fig. 5. The changes of Gibbs free energy for adsorption of benzotriazole, 2-mercaptobenzothiazole, 8-hydroxyquinoline, and 3-amino-1,2,4-triazole-5-thiol as corrosion inhibitors on the Al–Mg–Ge alloy surface in NaCl solution at 300 K.

surface. In fact, comparison to ΔG°_{ads} amounts confirmed a good agreement among calculated results, as well as the correctness of the selected isotherm for the adsorption process of benzotriazole → Al–Mg–Ge, 2-mercaptobenzothiazole → Al–Mg–Ge, 8-hydroxyquinoline → Al–Mg–Ge, and 3-amino-1,2,4-triazole-5-thiol → Al–Mg–Ge (Fig. 5).

The adsorptive capacity of inhibitor structures on the Al–Mg–Ge alloy surface is approved by the ΔG°_{ads} amounts:

$$\Delta G^{\circ}_{ads} = \left(\Delta G^{\circ}_{inh \to [Al\text{–}Mg\text{–}Ge]}\right) - \left(\Delta G^{\circ}_{inh} + \Delta G^{\circ}_{[Al\text{–}Mg\text{–}Ge]}\right). \quad (5)$$

On the basis of data in Table 1, it is predicted that the adsorption of the inhibitor on the Al–Mg–Ge alloy surface might be physical and chemical nature. As shown in Fig. 5, all the computed ΔG°_{ads} amounts are very close, which exhibit the agreement of the evaluated data by all methods and the validity of the computations and it has been also represented the maximum fluctuation for benzotriazole → Al–Mg–Ge, 2-mercaptobenzothiazole → Al–Mg–Ge, 8-hydroxyquinoline → Al–Mg–Ge, and 3-amino-1,2,4-triazole-5-thiol → Al–Mg–Ge, respectively (Fig. 5). Moreover, 2-mercaptobenzothiazole → Al–Mg-Ge has shown a sharpest peak in ΔG°_{ads} amount which displays the most stability in the coating process of the Al–Mg–Ge alloy surface with 2-mercaptobenzothiazole.

The heterocyclic organic inhibitors of benzotriazole, 2-mercaptobenzothiazole, 8-hydroxyquinoline, and 3-amino-1,2,4-triazole-5-thiol have approximately shown the identical behavior (20–2000 ppm) for various atoms in the active sites of these compounds through the nuclear magnetic resonance (NMR) properties (Fig. 6).

The sharpest peak of NMR spectrum has been almost observed between 20 ppm for these compounds. The weakest peaks of NMR spectrum have approximately appeared in 400–1000 ppm for all four heterocyclic organic inhibitors containing benzotriazole, 2-mercaptobenzothiazole, 8-hydroxyquinoline, and 3-amino-1, 2, 4-triazole-5-thiol adsorbed on the Al–Mg–Ge alloy surface (Fig. 6).

Then, the atomic charge and NMR data of isotropic (σ_{iso}) and anisotropic shielding tensor (σ_{aniso}) for benzotriazole → Al–Mg–Ge, 2-mercaptobenzothiazole→ Al–Mg–Ge, 8-hydroxyquinoline → Al–Mg–Ge, and 3-amino-1,2,4-triazole-5-thiol → Al–Mg–Ge have been calculated using Gaussian 16 revision C.01 software [39] and reported in Table 2.

The quantum chemical calculations yield the CS tensors in principal axes system to evaluate the isotropic chemical-shielding (CSI), anisotropic chemical-shielding (CSA) [54]:

$$\mathrm{CSI}\,(\mathrm{ppm}) = (\sigma 33 + \sigma 22 + \sigma l1)/3, \quad (6)$$

$$\mathrm{CSA}\,(\mathrm{ppm}) = \sigma 33 - (\sigma 22 + \sigma l1)/2. \quad (7)$$

The calculation of nuclear magnetic resonance (NMR) for chemical shifts for assigning the structural and geometrical of compounds has been accomplished. In fact, Gauge Invariant Atomic Orbital (GIAO) method has been suggested as an accurate method for NMR parameter calculations, and ONIOM has obtained much attention for achieving NMR chemical shifts in inhibitor-surface complexes, for instance, isotropic chemical shielding becomes:

$$\sigma_{iso,\,ONIOM} = \sigma_{iso,\,high(QM1)} + \sigma_{iso,\,medium(QM2)} + \sigma_{iso,\,low(QM3)}. \quad (8)$$

Besides, the solution of NaCl solution has influenced on the nuclear magnetic resonance data and chemical shielding of carbon, nitrogen, oxygen, sulfur, aluminum, magnesium and germanium in benzotriazole → Al–Mg–Ge, 2-mercaptobenzothiazole → Al–Mg–Ge, 8-hydroxyquinoline → Al–Mg–Ge, and 3-amino-1,2,4-triazole-5-thiol → Al–Mg–Ge. In Fig. 7, it has been indicated the chemical shielding tensors of isotropic (σ_{CSI}) and anisotropic (σ_{CSA}) of some effective atoms in the adsorption site of benzotriazole → Al–Mg–Ge, 2-mercaptobenzothiazole → Al–Mg–Ge, 8-hydroxyquinoline → Al–Mg–Ge, and 3-amino-1,2,4-triazole-5-thiol → Al–Mg–Ge (Table 2). Figure 7 has certainly has focused on the aluminum shielding in the intra-atomic interaction with magnesium, germanium and simultaneously interatomic interaction with other atoms in organic inhibitors through variety of high, medium and low layers of ONIOM method.

Interatomic interactions which is related position of one, two, three, etc. atoms at a time is written as a

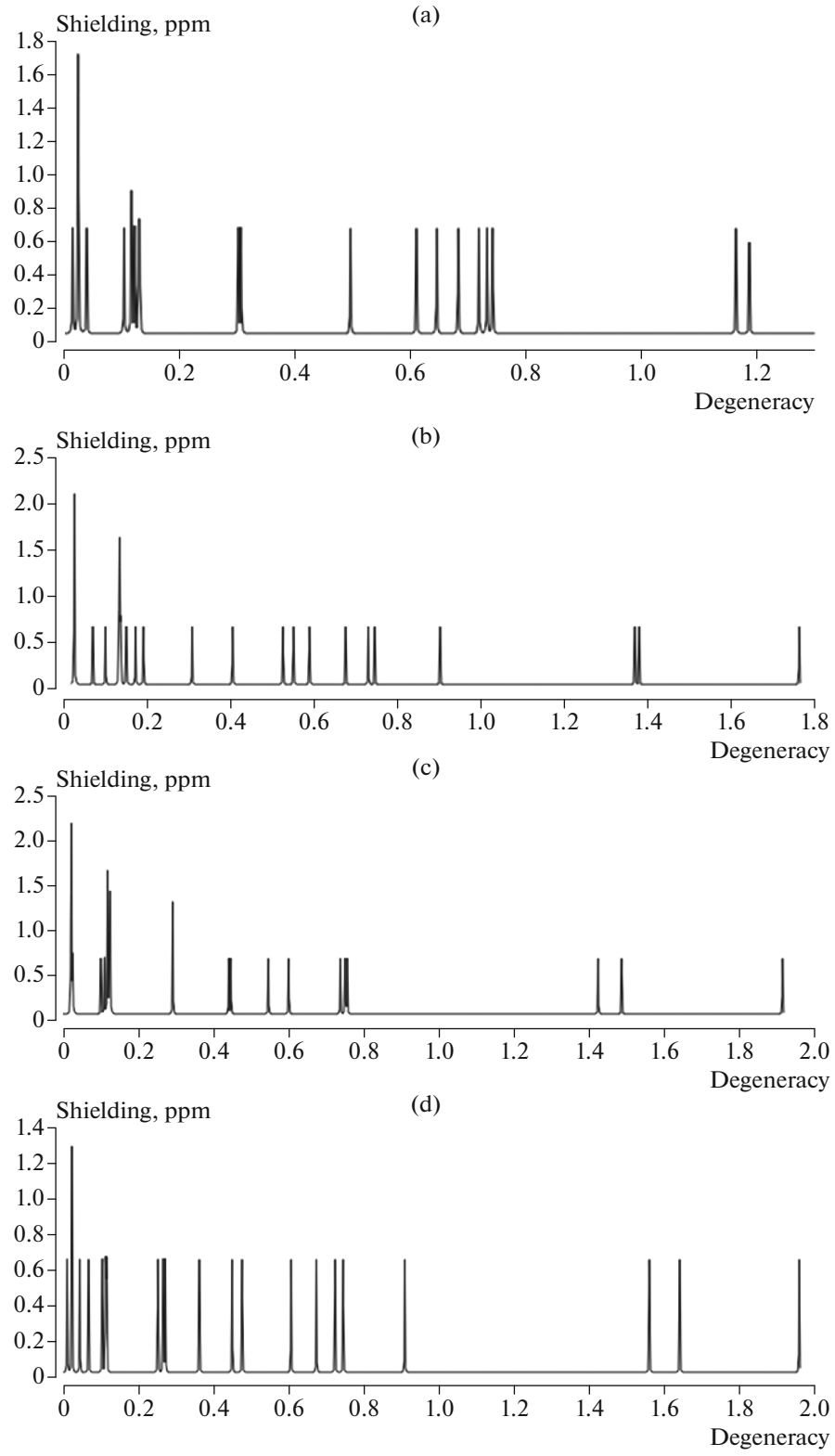

Fig. 6. Chemical shift of NMR spectroscopy for (a) benzotriazole → Al–Mg–Ge, (b) (2-mercaptobenzothiazole → Al–Mg–Ge, (c) 8-hydroxyquinoline → Al–Mg–Ge, and (d) 3-amino-1,2,4-triazole-5-thiol → Al–Mg–Ge; through the Langmuir adsorption process by indicating the active nitrogen,oxygen and sulfur atoms in heterocyclic compounds becoming close to the nanosurface.

Table 2. Atomic charge and NMR properties of some atoms of benzotriazole, 2-mercaptobenzothiazole, 8-hydroxyquinoline, and 3-amino-1,2,4-triazole-5-thiol in ppm adsorbed onto Al–Mg–Ge alloys surface

Atom number	Benzotriazole → Al–Mg–Ge			2-mercaptobenzothiazole → Al–Mg–Ge			8-hydroxyquinoline → Al–Mg–Ge			3-amino-1,2,4-triazole-5-thiol → Al–Mg–Ge		
	σ_{CSI}	σ_{CSA}	Q	σ_{CSI}	σ_{CSA}	Q	σ_{CSI}	σ_{CSA}	Q	σ_{CSI}	σ_{CSA}	Q
C1	117.97	130.99	−0.04	136.00	122.71	0.00	103.66	98.30	0.09			
C2	117.28	148.49	−0.01	133.57	132.94	−0.01	128.59	125.53	−0.02	109.97	96.56	0.22
C3	131.98	134.04	0.02	149.85	98.93	−0.23	120.98	121.13	0.04	118.35	94.08	0.00
C4	105.01	55.30	0.04	133.79	90.22	0.07	126.82	157.48	−0.01			
C5	130.30	128.27	0.01	134.26	130.35	0.01	128.32	120.99	−0.02			
C6	123.38	127.30	−0.01	132.20	133.20	−0.01	121.43	140.67	−0.00			
C8				99.83	83.21	−0.21	113.40	119.92	0.08			
S7				675.26	262.57	0.49				367.69	406.55	0.23
N8	−12.16	136.20	−0.08									
N9	40.28	309.41	−0.16	69.65	348.20	−0.28						
N10												
A110	611.25	568.10	0.12									
A111				404.53	1291.32	0.10						
A115				525.25	578.63	0.14						
A116	719.27	631.69	−0.62				449.15	912.81	0.11	678.53	1012.68	−0.10
A117				901.90	547.86	−0.91						
A118	496.93	1642.23	−0.16				740.12	642.32	−0.52			
A119				588.79	748.09	−0.14				611.31	1077.83	−0.07
A121	646.52	953.75	−0.15									
A122				550.50	877.35	−0.12						
A123							603.04	953.29	−0.16			
Mg9										728.24	281.15	−0.02
Mg11	733.47	285.98	−0.03							257.77	549.06	0.11
Mg12				744.93	404.04	0.03						
Mg13	307.50	526.50	0.18				758.94	355.43	−0.05	749.57	169.94	−0.10
Mg14				307.63	524.94	0.12						
Mg15	743.09	281.90	−0.02				294.82	625.41	0.14			
Mg16				729.70	364.53	−0.03						
Mg17							752.91	382.07	−0.02			
Mg18										271.76	541.36	0.149
Mg20	302.83	814.17	0.14									
Mg21				190.90	684.01	0.14						
Mg22							294.84	593.20	0.11			
Ge14							1425.78	1385.08	0.35			
Ge15										1960.66	1454.32	0.03
Ge17	2189.91	2513.66	0.21							1562.77	963.44	0.32
Ge18				1762.50	1796.59	0.13						
Ge19	1187.58	2180.36	0.29				1916.14	1722.89	0.19			
Ge20				1368.39	1405.73	0.30						
Ge21							1488.16	1260.09	0.28			

series expansion of functional parameters with interatomic potential [55]:

$$V = \sum_{i=1}^{N} V_1(\mathbf{r}_i) + \sum_{i,j=1}^{N} V_2(r_i, r_j) + \sum_{i,j,k=1}^{N} V_3(\mathbf{r}_i, \mathbf{r}_j, \mathbf{r}_k) + \ldots, \quad (9)$$

where V_1 is the one-body term, V_2 the two-body term, V_3 the three body term, N the number of atoms in the system, $\mathbf{r}_i$ the position of atom i, $\mathbf{r}_j$ the position of atom j, the position of atom k and i,j,k are indices that sprain around atom positions.

In Fig. 7, it has been presented that the isotropic and anisotropy shielding increase with the occupancy and consequently the negative charge of nitrogen, oxygen and sulfur atoms in benzotriazole, 2-mercaptobenzothiazole, 8-hydroxyquinoline, and 3-amino-1,2,4-triazole-5-thiol diffusing onto Al–Mg–Ge alloy surface. It has been exhibited that the graph of nitrogen, oxygen and sulfur atoms has the same attitude but a considerable deviation from carbon and hydrogen atoms.

Intra-atomic interactions consist of Al–Al, Al–Mg, Al–Ge, Mg–Mg, Mg–Ge, Ge-Ge and interatomic interaction are N → Al–Mg–Ge, O → Al–Mg–Ge, S → Al–Mg–Ge based on the of CAM-B3LYP/6-31+G(*d*, *p*)/EPR-III/LAN2DZ quantum

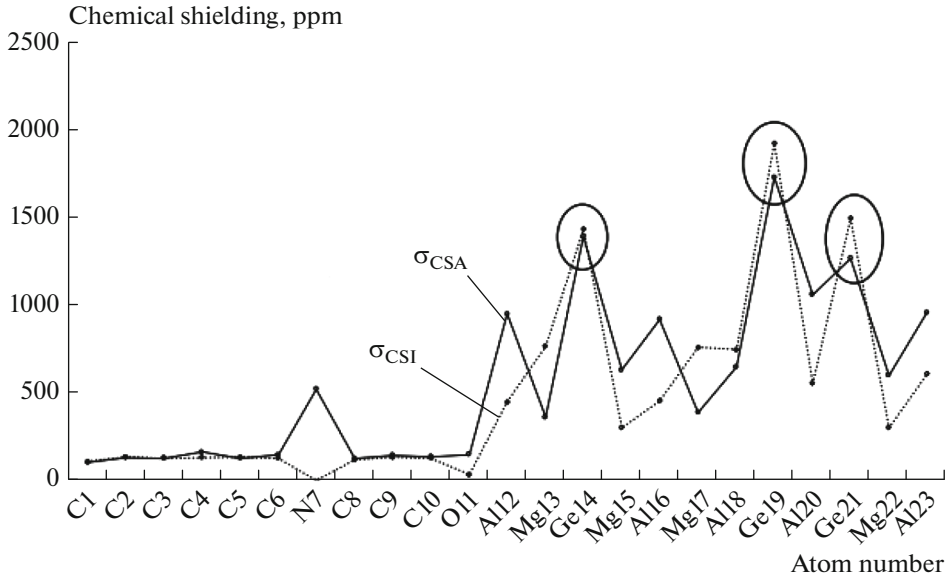

Fig. 7. The NMR plot of isotropic (σ_{iso}) and anisotropic (σ_{aniso}) shielding tensors for aluminum through intra-atomic interaction with magnesium and germanium atoms in alloy surface of Al–Mg–Ge and interatomic interaction with organic inhibitors in the adsorption site of (N → Al, O → Al, S → Al) calculated by level of theory CAM-B3LYP/6-31+G(*d*, *p*)/EPR-III/LANL2DZ.

mechanics calculations using Gaussian 16 revision C.01 program (Fig. 7).

Based on Fig. 7, it has been observed that Al–Ge(14), Al-Ge(19) and Al–Ge(21) direct us to the most influence in the neighbor atoms generated by interatomic reactions of N → Al, O → Al, S → Al in the Al–Mg–Ge alloy surface.

Nuclear quadrupole resonance (NQR) frequency for benzotriazole → Al–Mg–Ge, 2-mercaptobenzothiazole → Al–Mg–Ge, 8-hydroxyquinoline → Al–Mg–Ge, and 3-amino-1,2,4-triazole-5-thiol Al–Mg–Ge is proportional to the product of the nuclear quadrupole moment, a property of the nucleus, and the EFG in the neighborhood of the nucleus. As the EFG at the position of the nucleus in organic inhibitors is assigned by the valence electrons twisted in the special linkage with close nuclei of aluminum surface, the NQR frequency at which transitions happen is particular for an inhibitor→ metal alloy complex (Table 2). In NMR, nuclei with spin ≥1/2 have a magnetic dipole moment so that their energies are split by a magnetic field, permitting resonance sorption of energy dependent on the Larmor frequency; $\omega_L = \gamma B$, where γ is the gyromagnetic ratio and B is the magnetic field external to the nucleus.

In NQR, nuclei with spin ≥1, there is an electric quadrupole moment which is accompanied with nonspherical nuclear charge distributions. So, the nuclear charge distribution deviates from that of a sphere as the oblate or prolate form of the nucleus [56, 57].

NQR is a straight frame of the interaction of the quadrupole moment with the local electric field gradient (EFG) which is produced by the electronic structure of its ambiance. Therefore, the NQR transition frequencies are symmetric to the electric quadrupole moment of the nucleus and a measure of the strength of the local EFG: $\omega \sim \frac{e^2 Qq}{\hbar} = C_q$, where q is dependent on the biggest fundamental portion of the EFG tensor at the nucleus, and C_q is quadrupole coupling constant parameter [54, 55].

The NQR method is based on the multipole expansion in Cartesian coordinates as the following equations:

$$V(r) = V(0) + \left[\left(\frac{\partial V}{\partial x_i}\right)_0 . x_i\right] + \frac{1}{2}\left[\left(\frac{\partial^2 V}{\partial x_i x_j}\right)_0 . x_i x_j\right] + \ldots \quad (10)$$

Then, after simplification the equation, there are only the second derivatives dependent on the same variable for the potential energy [54, 55]:

$$U = -\frac{1}{2}\int_{\mathcal{D}} d^3 r \rho_r \left[\left(\frac{\partial^2 V}{\partial x_i^2}\right)_0 x_i^2\right] = -\frac{1}{2}\int_{\mathcal{D}} d^3 r \rho_r \left[\left(\left|\frac{\partial E_i}{\partial x_i}\right|_0 x_i^2\right)\right] = -\frac{1}{2}\left(\frac{\partial E_i}{\partial x_i}\right)_0 \int_{\mathcal{D}} d^3 r \left[\rho(r) x_i^2\right]. \quad (11)$$

There are two parameters which must be gotten from NQR experiments; the quadrupole coupling constant, χ, and asymmetry parameter of the EFG tensor η:

$$\chi = e^2 Q q_{zz}/h, \quad (12)$$

$$\eta = (q_{xx} - q_{yy})/ q_{zz}, \quad (13)$$

Table 3. The electric potential for elements of benzotriazole, 2-mercaptobenzothiazole, 8-hydroxyquinoline, and 3-amino-1,2,4-triazole-5-thiol adsorbed on the Al–Mg–Ge alloy surface by CAM-B3LYP/EPR-III, 6-31+G(*d*, *p*) calculation extracted of NQR method

Atom type	Benzotriazole	2-Mercaptobenzothiazole	8-Hydroxyquinoline	3-Amino-1,2,4-triazole-5-thiol
C1	−14.61	−14.55	−14.50	
C2	−14.57	−14.56	−14.57	−14.48
C3	−14.53	−14.56	−14.53	−14.54
C4	−14.54	−14.53	−14.55	
C5	−14.56	−14.56	−14.58	
C6	−14.57	−14.56	−14.56	
N4				−18.04
N5				−18.16
N6				−18.05
N8	−18.08			
N9	−18.09	−18.13		
S7		−58.27		−58.34
A18				−43.70
A110	−43.70			
A114	−43.68			−43.19
A116	−43.21		−43.70	−43.50
A118	−43.51		−43.21	
A121	−43.53			
A123			−43.52	
Mg9				−38.66
Mg11	−38.66			−38.90
Mg13	−38.89		−38.67	−38.63
Mg15	−38.67		−38.91	
Mg18				−38.91
Mg20	−38.88			
Mg22			−38.92	

where q_{ii} are components of the EFG tensor at the quadrupole nucleus determined in the EFG principal axes system, Q the nuclear quadrupole moment, e the proton charge and h is the Planck's constant [58]. In this article, the electric potential as the amount of work energy through transferring the electric charge from one site to another site in presence of electric field has been measured for benzotriazole, 2-mercaptoben zothiazole, 8-hydroxyquinoline, and 3-amino-1,2,4-triazole-5-thiol diffusing onto Al–Mg–Ge alloy surface using CAM-B3LYP/EPR-III/LANL2DZ/6-31+G(*d*, *p*) level of theory (Table 3).

The electric potential (J C^{-1}) is a continuous function in space produced by an idealized point charge has $1/r$ potential:

$$V_E = \frac{1}{4\pi\varepsilon_0}\frac{Q}{r},$$

where Q (measured in coulombs) is the point charge, r is the distance from the charge and ε_0 is the permittivity of vacuum.

Since the electric potential for a system of point charges is equal to the sum of the point charges' individual potentials, the calculations are done simply based on summation of potential fields which is scalar instead of summation of the electric fields which is vector and much more difficult that potential field. So,

$$V_E(r) = \frac{1}{4\pi\varepsilon_0}\sum_i \frac{q_i}{|r - r_i|},$$

where r is a point at which the potential is measured, r_i is a point at which the charge is $\neq 0$, and q_i is the charge at the point r_i. Finally, the potential of a continuous charge distribution $\rho(r)$ appears:

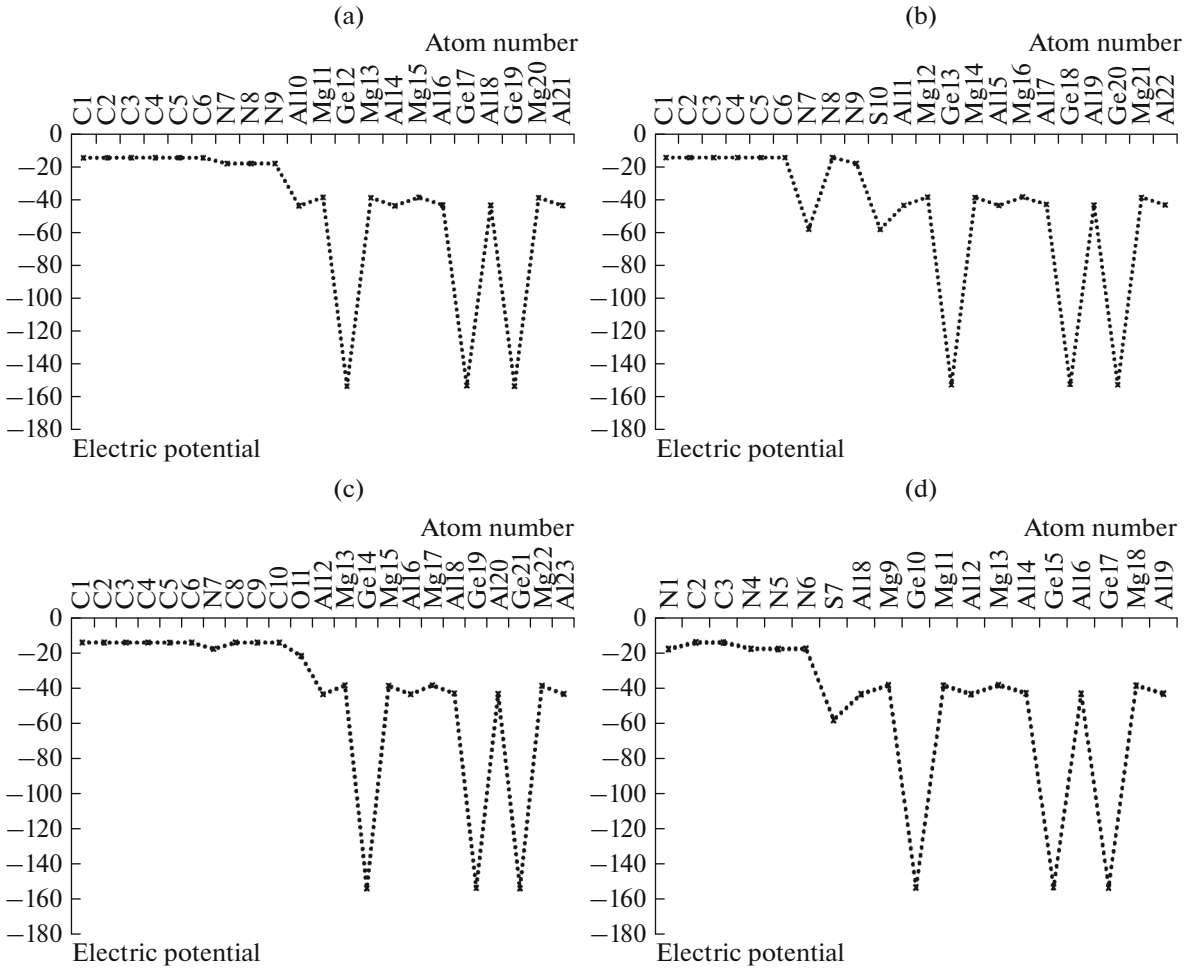

Fig. 8. The electric potential versus atom number through NQR calculation for (a) benzotriazole, (b) 2-mercaptobenzothiazole, (c) 8-hydroxyquinoline, and (d) 3-amino-1,2,4-triazole-5-thiol adsorbing on the Al–Mg–Ge alloy surface using CAM-B3LYP/EPR-III/LANL2DZ/6-31+G(*d*, *p*).

$$V_E(r) = \frac{1}{4\pi\varepsilon_0}\int_R \frac{\rho(r')}{|r-r'|}\, d^3r',$$

where R is a region including all the points at which the charge density is $\neq 0$, r' is a point inside R, and $\rho(r')$ is the charge density at the point r' [59].

In addition, in Fig. 8, it has been plotted the electric potential of NQR method for elements of benzotriazole, 2-mercaptobenzothiazole, 8-hydroxyquinoline, and 3-amino-1,2,4-triazole-5-thiol that have been adsorbed on the Al–Mg–Ge alloy surface using CAM-B3LYP/EPR-III/LANL2DZ/6-31+G(*d*, *p*) level of theory.

Therefore, it has been observed the effect of the replacement of Al elements in Al–Al surface with magnesium and germanium through resulted electric potential using NQR analysis (Fig. 8). It's obvious that the graph of Al–Al is fluctuated by Mg and Ge atoms in the related alloy. In Fig. 8, it has been remarked the changes of electric potential for carbon, nitrogen, oxygen, sulfur, aluminum, magnesium, and germanium in benzotriazole → Al–Mg–Ge, 2-mercaptobenzothiazole → Al–Mg–Ge, 8-hydroxyquinoline → Al–Mg–Ge, and 3-amino-1,2,4-triazole-5-thiol → Al–Mg–Ge.

Finally, the charge density (Table 2) has shown a more important charge transfer from nitrogen, oxygen and sulfur of benzotriazole, 2-mercaptobenzothiazole, 8-hydroxyquinoline and 3-amino-1,2,4-triazole-5-thiol as the electron donor adsorbed onto Al–Mg–Ge nanoalloy surface which acts as the electron acceptor (N → Al, O → Al and S → Al). As a matter of fact, Al sites in Al–Mg–Ge nanoalloy surface have higher interaction energy from Van der Waals' forces with these heterocyclic inhibitors that can make them highly stable toward coating information on the surface.

It has been predicted that the priority for selecting the surface binding of nitrogen, oxygen and sulfur of these heterocyclic inhibitors in adsorption sites can be

affected by the presence of close atoms of magnesium and germanium in the Al–Mg–Ge nanoalloy surface.

CONCLUSIONS

In this research, the competence of nitrogen and sulfur heterocyclic inhibitors as the ternary Al–Mg–Ge nanoalloy surface coating has been investigated through the thermoelectric traits and specifications of the environmental condition. Therefore, the spectroscopy of NMR, NQR, IR, PDOS has been accomplished for achieving parameters of chemical shielding, electric potential, charge distribution, thermodynamic properties, projection density of states and other quantum data extracted from benzotriazole → Al–Mg–Ge, 2-mercaptobenzothiazole → Al–Mg–Ge, 8-hydroxyquinoline → Al–Mg–Ge, and 3-amino-1,2,4-triazole-5-thiol → Al–Mg–Ge complexes.

An elaborate investigation for the mechanism of local minima in the adsorption potential energy landscape represents that the intact benzotriazole, 2-mercaptobenzothiazole, 8-hydroxyquinoline, and 3-amino-1,2,4-triazole-5-thiol have been adsorbed with the aromatic ring parallel to the Al–Mg–Ge alloy surface.

In the preferred path, these nitrogen and sulfur heterocyclic inhibitors remain parallel to the surface while performing small single rotational steps with a carbon-carbon double bond hinged above a single aluminum atom in Al–Mg–Ge surface. The most eventual adsorption state of the inhibitors is one in which nitrogen or sufur atom of aromatic ring moves toward the aluminum atom in Al–Mg–Ge surface in an inclined state.

ACKNOWLEDGMENTS

In successfully completing this paper and its research, the authors are grateful to Kastamonu University for their support through the library, the laboratory, and scientific websites.

CONFLICT OF INTEREST

The authors declare that they have no conflicts of interest.

REFERENCES

1. E. Machnikova, K. H. Whitmire, N. Hackerman, et al., Electrochim. Acta **53**, 6024 (2008). https://doi.org/10.1016/j.electacta.2008.03.021
2. M. Benabdellah, R. Touzani, A. Aouniti, et al., Mater. Chem. Phys. **105**, 373 (2007). https://doi.org/10.1016/j.matchemphys.2007.05.001
3. A. Fiala, A. Chibani, A. Darchen, et al., Appl. Surf. Sci. **253**, 9347 (2007). https://doi.org/10.1016/j.apsusc.2007.05.066
4. A. Tahan, F. Mollaamin, and M. Monajjemi, Russ. J. Phys. Chem. **A83**, 587 (2009). https://doi.org/10.1134/S003602440904013X
5. M. Liu, C. D. Marioara, R. Holmestad, et al., Mater. Sci. Forum **794–796**, 971 (2014). doi 10.4028/www.scientific.net/MSF.794-796.971
6. P. R. Vasyutin, E. A. Lagunova, M. Y. Sinev, et al., Russ. J. Phys. Chem. B **16**, 1231 (2022). https://doi.org/10.1134/S1990793122070168
7. P. R. Vasyutin, Y. A. Gordienko, M. Y. Sinev, et al., Russ. J. Phys. Chem. B **16**, 1259 (2022), https://doi.org/10.1134/S199079312207017X
8. N. A. Kochetov, Russ. J. Phys. Chem. B **16**, 621 (2022). https://doi.org/10.1134/S1990793122040078
9. K. Xu, Y. Cui, Y. Yu, et al., Russ. J. Phys. Chem. B **16**, 787 (2022). https://doi.org/10.1134/S1990793122040054
10. A. V. Dubovik, Russ. J. Phys. Chem. B **15**, 696 (2021). https://doi.org/10.1134/S1990793121040151
11. A. A. Voznyakovsky, A. P. Wozniakovsky, S. V. Kidalov, et al., Russ. J. Phys. Chem. B **15**, 377 (2021). https://doi.org/10.1134/S1990793121030325
12. F. Lasagni, A. Lasagni, E. Marks, et al., Acta Mater. **55**, 3875 (2007). https://doi.org/10.1016/j.actamat.2007.03.004
13. G. Requena, G. Garcés, M. Rodríguez, et al., Adv. Eng. Mater. **11**, 1007 (2009). https://doi.org/10.1002/adem.200900218
14. Z. Asghar, G. Requena, and F. Kubel, Mater. Sci. Eng. A **527**, 5691 (2010). https://doi.org/10.1016/j.msea.2010.05.033
15. F. Stadler, H. Antrekowitsch, W. Fragner, et al., Int. J. Cast. Metals Res. **25**, 215 (2012). https://doi.org/10.1179/1743133612Y.0000000004
16. Y. Boughoues, M. Benamira, L. Messaadia, et al., Eng. Asp. **593**, 124610 (2020). https://doi.org/10.1016/j.colsurfa.2020.124610
17. M. Özcan, R.Solmaz, G. Kardaş, et al., Eng. Asp. **325**, 57 (2008). doi 10. 1016/j.colsurfa.2008.04.031
18. J. Saranya, M. Sowmiya, P. Sounthari, et al., J. Mol. Liq. **216**, 42 (2016). https://doi.org/10.1016/j.molliq.2015.12.096
19. T. A. S. Guimarães, J. N. da Cunha, G. A. de Oliveira, et al., J. Mater. Res. Technol. **9**, 7104 (2020). https://doi.org/10.1016/j.jmrt.2020.05.019
20. M. Ozcan, Acta Phys.-Chim. Sin. **24**, 1387 (2008). https://doi.org/10.1016/S1872-1508(08)60059-5
21. M. Mobin and R. Aslam R. Process Saf. Environ. Prot. **114**, 279 (2018). https://doi.org/10.1016/j.psep.2018.01.001
22. M. Monajjemi, M. Khaleghian, N. Tadayonpour, et al., Int. J. Nanosci. **09**, 517 (2010). https://doi.org/10.1142/S0219581X10007071
23. S. A. Ali, M. A. J. Mazumder, M. K. Nazal, et al., Arab. J. Chem. **13**, 242 (2020). https://doi.org/10.1016/j.arabjc.2017.04.005
24. M. Monajjemi, M. T. Baie, and F. Mollaamin, Russ. Chem. Bull. **59**, 886 (2010). https://doi.org/10.1007/s11172-010-0181-5

25. E.-S. M. Sherif, H. S. Abdo, K. A. Khalil, et al., Metals **5**, 1799 (2015). https://doi.org/10.3390/met5041799

26. E. S. Sherif, Molecules **19**, 9962 (2014). https://doi.org/10.3390/molecules19079962

27. D. Yang, M. Zhang, J. Zheng, et al., RSC Adv. **5**, 95160 (2015). https://doi.org/10.1039/ C5RA14556B

28. M. Finšgar and I. Milošev, Corros. Sci. **52**, 2737 (2010). https://doi.org/10.1016/j.corsci.2010.05.002

29. A. Y. Shen, S. N. Wu, and C. T. Chiu, J. Pharm. Pharmacol. **51**, 543 (1999). https://doi.org/10.1211/0022357991772826

30. P. A. J. Cabassi, B. K. Loveday, Ph. Radcliffe, et al., J. South African Inst. Mining Metall. **83**, 270 (1983).

31. M. Monajjemi, F. Mollaamin, M. R. Gholami, et al., Main Group Met. Chem. **26**, 349 (2003). https://doi.org/10.1515/MGMC.2003.26.6.349

32. F. Mollaamin, S. Shahriari, M. Monajjemi, et al., J. Clust. Sci. **34**, 1547 (2023). https://doi.org/10.1007/s10876-022-02335-1

33. F. Mollaamin and M. Monajjemi, Mol. Simul. **49**, 365 (2023). https://doi.org/10.1080/08927022.2022.2159996

34. M. E. Mashuga, L. O. Olasunkanmi, and E. E. Ebenso, J. Mol. Struct. **1136**, 127 (2017). https://doi.org/10.1016/j.molstruc.2017.02.002

35. Y. Jing, J. Zhang, W. Hu, et al., Russ. J. Phys. Chem. B **15**, S102 (2021). https://doi.org/10.1134/S1990793121090165

36. M. Svensson, S. Humbel R. D. J. Froese, et al., J. Phys. Chem. **100**, 19357 (1996). https://doi.org/10.1021/jp962071j

37. F. Brandt and C. R. Jacob, Systematic **18**, 2584 (2022). https://doi.org/10.1021/acs.jctc.1c01093

38. R. Dennington, T. A. Keith, and J. M. Millam, *Gauss-View, Version 6* (Semichem Inc., Shawnee Mission, KS, 2016).

39. M. J. Frisch, G. W. Trucks, H. B. Schlegel, G. E. Scuseria, M. A. Robb, J. R. Cheeseman, G. Scalmani, V. Barone, G. A. Petersson, H. Nakatsuji, X. Li, M. Caricato, A. V. Marenich, J. Bloino, B. G. Janesko, et al., *Gaussian 16, Revision C.01* (Gaussian, Inc., Wallingford, CT, 2016).

40. Z. Wu, L. Zhang, and Y. Liao, Russ. J. Phys. Chem. B **15**, S81 (2021). https://doi.org/10.1134/S1990793121090153

41. O. N. Fedyaeva and A. A. Vostrikov, Russ. J. Phys. Chem. B **16**, 1409 (2022). https://doi.org/10.1134/S1990793122080140

42. M. Monajjemi, M. Khaleghian, N. Tadayonpour, et al., Int. J. Nanosci. **9**, 517 (2010). https://doi.org/10.1142/S0219581X10007071

43. K. Bakhshi, F. Mollaamin, and M. Monajjemi, J. Comput. Theor. Nanosci. **8**, 763 (2011). https://doi.org/10.1166/jctn.2011.1750

44. T. Ravi and S. Sundararaman, Russ. J. Phys. Chem. B **15**, 462 (2021). https://doi.org/10.1134/S1990793121030295

45. F. Mollaamin, M. Monajjemi, S. Salemi, et al., Fuller. Nanotub. Carbon Nanostruct. **19**, 182 (2011). https://doi.org/10.1080/15363831003782932

46. A. D. Becke, J. Chem. Phys. **98**, 5648 (1993). https://doi.org/10.1063/1.464913

47. C. Lee, W. Yang, and R. G. Parr, Phys. Rev. B **37**, 785 (1988). https://doi.org/10.1103/PhysRevB.37.785

48. K. Kim and K. D. Jordan, J. Phys. Chem. **98**, 10089 (1994). https://doi.org/10.1021/j100091a024

49. P. J. Stephens, F. J. Devlin, C. F. Chabalowski, et al., J. Phys. Chem. **98**, 11623 (1994); https://doi.org/10.1021/j100096a001

50. C. J. Cramer, *Essentials of Computational Chemistry: Theories and Models*, 2nd ed. (John Wiley and Sons, New York, 2004).

51. S. H. Vosko, L. Wilk, M. Nusair, Can. J. Phys. **58**, 1200 (1980). https://doi.org/10.1139/p80-159

52. A. D. Becke, Phys. Rev. A **38**, 3098 (1988). https://doi.org/10.1103/PhysRevA.38.3098

53. R. Ditchfield, W. J. Hehre, and J. A. Pople, J. Chem. Phys. **54**, 724 (1971). https://doi.org/10.1063/1.1674902

54. R. A. Fry, K. D. Kwon, S. Komarneni, et al., Langmuir **22**, 9281 (2006). https://doi.org/10.1021/la061561s

55. M. Finnis, Prog. Mater. Sci. **52**, 133 (2007). https://doi.org/10.1016/j.pmatsci.2006.10.003

56. J. A. S. Smith, J. Chem. Educ. **48**, 39 (1971). https://doi.org/10.1021/ed048p39

57. A. N. Garroway, J. B. Miller, and M. L. Buess, "Explosives detection by pure 14N NQR," in *Proceedings of the 1st International Symposium on Explosive Detection Technology, Atlantic City, USA* (November 13–15, 1991).

58. O. Kh. Poleshchuck, E. L. Kalinna, and J. N. Latosinska, J. Koput, J. Mol. Struct. **547**, 233 (2001).

59. H. A. Young, R. D. Freedman, *Sears and Zemansky's University Physics with Modern Physics*, 13th ed. (Addison-Wesley, Boston, 2012), p. 754.